J Nanopart Res (2020) 22:242
https://doi.org/10.1007/s11051-020-04973-w

RESEARCH PAPER

# A nonparabolic conduction band study of circular quantum dot optical properties: modeling of surface roughness by using Koch snowflakes

**M. Solaimani** · **Abdolreza Rasouli Kenari**

Received: 28 March 2020 / Accepted: 3 August 2020


**Abstract** In this work, we investigate the optical properties of single and multiple quantum dots (QDs) based on $Al_xGa_{1-x}As/GaAs$ with two Koch snowflake-shaped and circular geometries. The idea is to determine the impact of the surface roughness of the circular QDs on the mentioned optical properties. This is an important issue in designing optoelectronic devices (e.g., photodetectors or light-emitting systems) because the position and magnitude of the absorption coefficient play important roles in devising them. We have also studied the effects of the conduction band nonparabolicity, QD size, number of QDs, and composition parameter $x$ on the absorption coefficient. For this purpose, we have used an efficient finite difference method to solve the two-dimensional Schrodinger equation. The computational algorithm of the Koch snowflake-shaped QD production is also described.

M. Solaimani (✉)
Department of Physics, Faculty of Science, Qom University of Technology, Qom, Iran
e-mail: solaimani@qut.ac.ir

A. R. Kenari
Faculty of Electrical and Computer Engineering, Qom University of Technology, Qom, Iran

*Present Address:*
M. Solaimani
Department of Physics, Faculty of Mechanical Engineering, Qom University of Technology, Qom, Iran

**Keywords** $Al_xGa_{1-x}As/GaAs$ Koch snowflake-shaped and circular single and multiple quantum dots (QDs) · Efficient finite difference method · Conduction band nonparabolicity · Nanostructures

## Introduction

Bulk semiconductor materials are potentially sensitive to absorb or emit a large portion of the electromagnetic spectrum. By reducing the carrier's confinement to three dimensions, the QDs generate and intersubband transitions are allowed. During the last few years, there has been a growing interest in the study of QDs. These structures behave like artificial atoms with outstanding optoelectronic properties. Nowadays, QDs have found vast applications in modern technologies such as amplifiers (Borri et al. 2000), photodetectors (Hellström et al. 2010), photodiode (Ji et al. 2008), memories (Nilsson et al. 2006), nanolasers (Gonzalez et al. 1999a), charge qubits (Hentschel et al. 2007), solar cells (Linares et al. 2011), transistors (Cervenka et al. 2011), and waveguides (Ma and John 2011). To make a better comparison between modern technologies with and without QDs especially in plasmonic devices, one can see Refs. (Gerislioglu et al. 2020a, b; Gerislioglu and Ahmadivand 2020).

The effect of conduction band nonparabolicity on the optical properties of semiconducting heterostructures has less been investigated. However, there are illustrative papers that investigate this issue (Riffe 2002) or reveal the effect of this parameter on the physical

Published online: 10 August 2020

properties of a quantum system. Influence of the nonparabolicity on the electronic structure of quantum cascade lasers (Vukovic et al. 2014) was studied by Vukovic et al., the effect of band nonparabolicity on the donor states in spherical QDs was investigated by Bose et al. (Bose et al. 2006), the effect of band nonparabolicity on mobility in a d-doped semiconductor was explored by Gonzalez group (Gonzalez et al. 1999b), and the effect of nonparabolicity on transition energy shift was considered by Le et al. (Le 2009).

So far, conical (RVNMelnik1 and Willatzen 2004), cubic (Khordada 2012), spherical (Solaimani et al. 2016), cylindrical (Solaimani 2016), lens-shaped (Rodrıguez and Ramırez 2008), and Y-shaped (Fang and Wang 2007) QDs have been investigated, and different methods have been implemented to solve the resulting Schrodinger equation such as finite element (Lin and Ho 2011), variational (Kervan et al. 2003), and density functional (Alemany et al. 2008) ones. However, the effect of the surface roughness of a round QD has not so far been studied. We want to address the experimental researchers' worry about the importance of the QDs' roundness in his/her research. However, we note that to have more realistic descriptions, we have to consider rough QD surfaces. The roughness effect is an inevitable result of epitaxial growth kinetics (Shokri and Ebrahiminejad 2011). The effect of roughness on different quantities such as dipolar interaction energy of two parallel planes (Vargas and Altbir 2000), conductance (Amado et al. 2005), spin-dependent tunneling (Shokri and Ebrahiminejad 2011), photoluminescence of gold (Yorulmaz et al. 2012), and electrical characteristics of silicon nanowire solar cells (Martinez et al. 2010) have so far been investigated. The importance of the roughness arises from the fact that the sources of the disorder can come from roughness at the heterojunctions (Amado et al. 2005). Surface roughness has a greater effect on the near-field than on the far-field (in optoelectronic devices), and slightly increases the vacuum Rabi splitting on average in quantum emitter-metallic nanoparticle systems (Lu et al. 2018). Up to our knowledge, most of the available papers on the roughness effect on the physical properties of nanostructures are devoted to quantum well systems. But our current work is devoted to the effect of the surface roughness of QDs on some physical properties. In one available paper on QDs, by using a complicated formalism, the authors tried to investigate the effect of the surface roughness on the optical properties of coupled-cavity photonic crystal waveguides (Fussell et al. 2008). In another work, it was shown that due to the interferences between reflections on different atomic planes, surface roughness generally decreases the valley splitting (Ibberson et al. 2018). But, can fractal structures account for the roughness effect of a physical quantity? Fractal patterns are natural phenomena that can be seen in nature such as trees, mountains, and seashells. Fractal structures have vast diversities of parameters, which by using them designing new optoelectronic devices with desired optical properties can be possible. So far, fractal structures have been used in different fields such as quantum transport in Sierpinski carpets (van Veen et al. 2016), scattering and diffraction from fractal objects (Allain and Cloitre 1986), enhancing the nonlinear optical response (Dutta Gupta 1998) (it is said that this enhancement can be due to the fractal geometry (Sankar and Philip 2018)), improvement of microelectronic nanodevices' applications (Chen et al. 2014), fractal antennas (Yazgan et al. 2015), and QD lasers (Liu et al. 2013). Also, fractal patterns can be fabricated by techniques such as annealing of nanoparticles and irradiation (Chen et al. 2014). Recently (Amini et al. 2017), we also considered the effect of the Fibonacci order on the optical properties of multiple quantum well systems.

In the present work, we have studied the optical properties of two-dimensional $Al_xGa_{1-x}As/GaAs$ single and multiple QDs with Koch snowflake shapes to answer the question about the roundness of the QDs we have mentioned above. The main idea was to determine the influence of the QD surface roughness on the optical properties. The reason to select the Koch snowflake is also that self-assembled nanodot arrays have a natural tendency to be formed in the fractal-like patterns (Eah 2011; Anghinolfi 2012; Jung et al. 2006). Besides, we have tried to evaluate the effect of the conduction

band nonparabolicity on the absorption coefficient. The paper has been organized as follows. In "Theory" section, we will describe the numerical Koch snowflake-shaped QD generation procedure, governing Hamiltonian, and an efficient finite difference method to solve the resulting Schrodinger equation. In "Finite difference scheme" section, we have interpreted the obtained results. Finally, in the last part, we have provided some concluding remarks.

## Theory

Physical properties of two-dimensionally confined electrons in snowflake shape Koch QDs can be obtained by using a two-dimensional Schrodinger equation (Bose et al. 2007),

$$\left[-\frac{\hbar^2}{2m^*}\nabla^2-\gamma\left(\frac{\hbar^2}{2m^*}\right)^2\nabla^4+V(x,y)\right]\psi(x,y) = E\psi(x,y); x,y\in\text{inside the QD} \quad (1-1)$$

$$\left[-\frac{\hbar^2}{2m^*}\nabla^2+V(x,y)\right]\psi(x,y) = E\psi(x,y); x,y\in\text{inside the QD} \quad (1-2)$$

where $m^* = (0.067 + 0.083x)m_0$ (Adachi 1985) and $\hbar$ are the effective mass of the electron and Planck constant, respectively. We define the geometrical Confining potential as $V(x, y) = 1.1x$ inside the QD, $V(x, y) = 0$outside the QD and inside the box, and $V(x, y) = \infty$ at other positions, where the value $1.1x$ is taken from Ref. (Adachi 1985). To evaluate the function$V(x, y)$, we have used the following procedure. Suppose that, we have a rectangular surface area of the size $L \times L$ which is divided into resolution points, as depicted in Fig. 1. Repeat these steps to draw a snowflake and find its vertices: (1) Compute the center of the rectangular surface as O. (2) Draw a circle with center O and the specified radius. (3) Find the three vertices of the equilateral triangle as △(A-B-C). (4) Compute the inscribed circle radius as 0.57 * Radius. // {Recursive Operation}. (5) Compute the 180° rotated triangle of △(A-B-C) as △(P-Q-R). (6) Divide each edge of △(A-B-C) into three segments and find the new vertices as AB1, AB2, AC1, AC2, BC1, and BC2. Then, repeat steps 5 and 6 for six new triangles △(A-AB1-AC1), △(B-AB2-BC1), △(C-AC2-BC2), △(P-BC1-BC2), △(Q-AC1-AC2), and △(R-AB1-AB2) in specified iteration times. Subsequently, by putting these snowflake-shaped QDs in a rectangular surface area of length L, we will study the optical properties of single and multiple QDs. After the numerical generation of the required potential profile, Eq. (1) where there is an eigenvalue problem on the rectangular space domain $\Omega = [a_x, b_x] \times [a_y, b_y]$ is ready to be solved. For this purpose, we have used a finite difference method to produce a matrix eigenvalue problem and find the energy spectrum and the corresponding wave functions.

Figure 1 shows the results for few iterations in the abovementioned algorithm.

## Finite difference scheme

By using the interpolation method, we generate finite difference coefficients. First, we equidistantly discretize the x-axis and find the function y = f (x) at these discrete points ($x_k$, $y_k = f(x_k)$), k = 0, 1, 2,. .., n-1. By using the Lagrange interpolating polynomials p(f, x) of the degree n-1, we writef (x) = $P_{n-1}(f, x) + R_{n-1}$, where we have $P_n(f, x) = \sum_k L_k(x) f(x_k)$. Also, the polynomials $L_k(x)$ of degree n-1 are the Lagrange interpolation coefficients: $L_k(x) = \prod_j (x - x_j) / (x_k - x_j)$. Then, we differentiate the Lagrange interpolation formula and evaluate the derivatives at the discretized points with equidistant interval $h$. Now, we can obtain the $m$th derivative of y = f(x) at $x_i$, i = 0, 1... n-1, as follows (Solaimani 2018):

$$\left(\left(\frac{d}{dx}\right)^m y\right)_i = \left(\frac{m!}{h^m}\right)\left(\frac{1}{(n-1)!}\sum_{j=0}^{n-1} mnA_{ij}y_j + {}_{mn}E_j\right) \quad (2)$$

where ${}_{mn}E_j$ are truncations errors. At this time, in the finite difference scheme, we approximate the second derivative in Eq. (1) by,

$$\nabla^2 f = \frac{\psi(x+h_x,y) - 2\psi(x,y) + \psi(x-h_x,y)}{{h_x}^2} + \frac{\psi(x,y+h_y) - 2\psi(x,y) + \psi(x,y-h_y)}{{h_y}^2} \quad (3)$$

And the fourth derivative as,

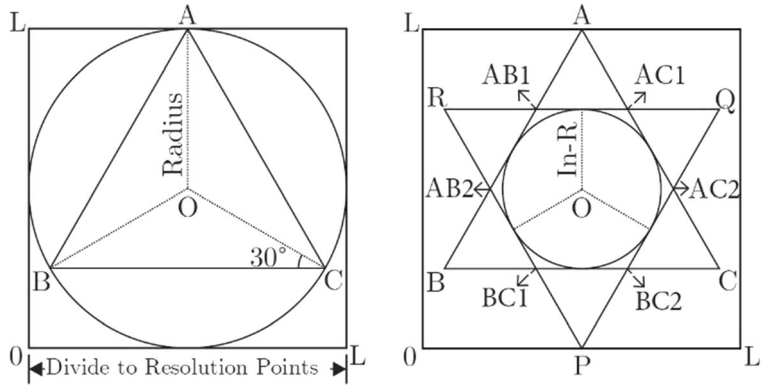


**Fig. 1** Presenting L; resolution; radius; in-radius; A, B, C; and their symmetric points P and Q

$$\nabla^4 f = \frac{\psi(x+2h_x,y)-4\psi(x+h_x,y)+6\psi(x,y)-4\psi(x-h_x,y)+\psi(x-2h_x,y)}{{h_x}^4} + 2\frac{\psi(x+h_x,y+h_y)-2\psi(x,y+h_y)+\psi(x-h_x,y+h_y)}{{h_x}^2\,{h_y}^2} - 4\frac{\psi(x+h_x,y)-2\psi(x,y)+\psi(x-h_x,y)}{{h_x}^2\,{h_y}^2} + 2\frac{\psi(x+h_x,y-h_y)-2\psi(x,y-h_y)+\psi(x-h_x,y-h_y)}{{h_x}^2\,{h_y}^2} + \frac{\psi(x+2h_y,y)-4\psi(x+h_y,y)+6\psi(x,y)-\psi(x-h_y,y)+\psi(x-2h_y,y)}{{h_y}^4} \tag{4}$$

By defining $\psi(x+ih_x, y+jh_y) = \psi_{i,j}$, $i,j = 0, \pm 1, \pm 2, \pm 3, \ldots$, we rewrite Eq. (1-1) as

$$-\gamma\left(\frac{\hbar^2}{2m^*}\right)^2\left\{\frac{\psi_{i+2,j}-4\psi_{i+1,j}+6_{i,j}-4\psi_{i-1,j}+\psi_{i-2,j}}{{h_x}^4} + 2\frac{\psi_{i+1,j+1}-2\psi_{i,j+1}+\psi_{i-1,j+1}}{{h_x}^2\,{h_y}^2} - 4\frac{\psi_{i+1,j}-2\psi_{i,j}+\psi_{i-1,j}}{{h_x}^2\,{h_y}^2} + 2\frac{\psi_{i+1,j-1}-2\psi_{i,j-1}+\psi_{i-1,j-1}}{{h_x}^2\,{h_y}^2} + \frac{\psi_{i+2,j}-4\psi_{i+1,j}+6\psi_{i,j}-\psi_{i-1,j}+\psi_{i-2,j}}{{h_y}^4}\right\} - \left(\frac{\hbar^2}{2m^*}\right)\left\{\frac{\psi_{i+1,j}-2\psi_{i,j}+\psi_{i-1,j}}{{h_x}^2} + \frac{\psi_{i,j+1}-2_{i,j}+\psi_{i,j-1}}{{h_y}^2}\right\} + V_{i,j}\psi_{i,j} = E\psi_{i,j} \tag{5}$$

If $N_x$ and $N_y$ are the number of discretization points along the x and y directions, then the resulting Hamiltonian matrix is a $(N_x \times N_y) \times (N_x \times Ny)$ one. Also, $\psi_{n,\ m}$is some $N_x \times N_y$ element vectors. These matrices yield a matrix eigenvalue problem. After calculation of the eigen-energies and eigenfunctions (Sabzevar et al. 2019), we have evaluated the linear absorption coefficient for ($E_f$–$E_i$) transition in the compact density matrix approach as (Solaimani et al. 2015),

$$\alpha^{(1)}(\omega) = \omega\sqrt{\frac{\mu}{\varepsilon_r}} \times \frac{\sigma_s e^2 \left|M_{fi}\right|^2 \hbar\Gamma_{fi}}{\left(\hbar\omega - \Delta E_{fi}\right)^2 + \left(\hbar\Gamma_{fi}\right)^2} \tag{6}$$

where $\omega$ is the frequency of the excitation electromagnetic field. $\sigma_s$represents electron density in this system, $E_i$ and $E_f$ denote the quantized energy levels for the initial and final states, respectively, $\mu$ is the permeability, and $\Gamma_{fi}(f \neq i)$ is the inverse

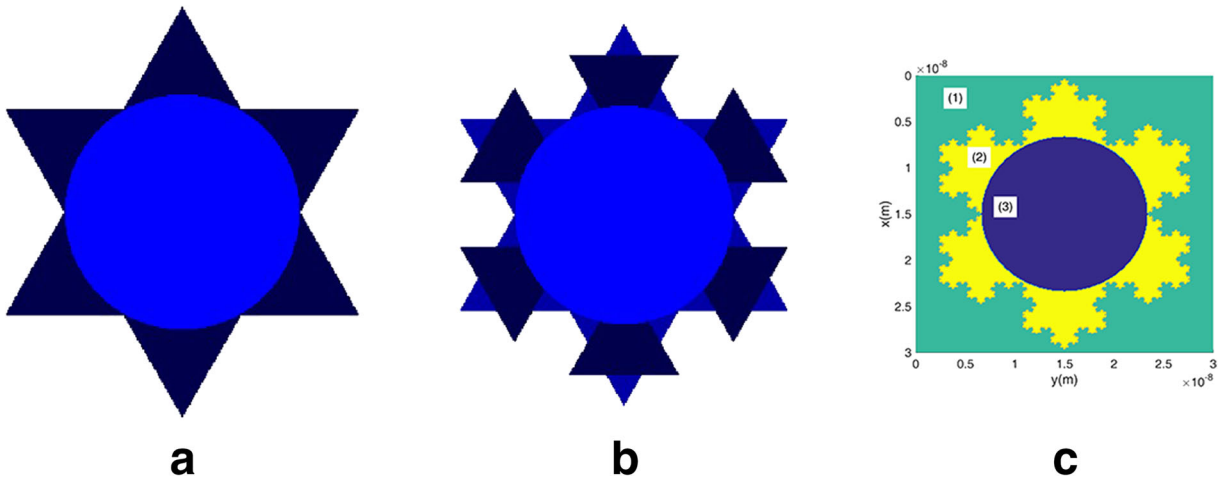


**Fig. 2** The result of snowflake generation by iteration = 1 (panel **a**) and 2 (panel **b**), respectively. In panel **c**, we have placed the snowflake in a rectangular box of length 30 nm

of relaxation time $T_{\mathrm{fi}}$ for states $|f\rangle$ and $|i\rangle$, namely $\Gamma_{fi} = 1/T_{fi}$. Finally, we evaluate the electric dipole moment transition matrix element $M_{fi} = \langle\psi_1|x|\psi_2\rangle$ for the x-polarization of the incident light (Kasapoglu et al. 2014).

## Results and discussions

In this paper, we have tried to model the effect of the surface roughness on the optical properties of single and multiple circular $Al_xGa_{1-x}As/GaAs$ QDs. For this purpose, we have used snowflake-shaped QDs and compared the optical absorption coefficients of the circular and snowflake-shaped QDs with the same radiuses. Besides, we have added the nonparabolicity effect and compared two cases existing and absenting of this effect. When the potential profile was generated, we have used a finite difference method to solve the two-dimensional Schrodinger equation and comprehensively presented its formulation in the last section. Then, by using the obtained energy eigenvalues and

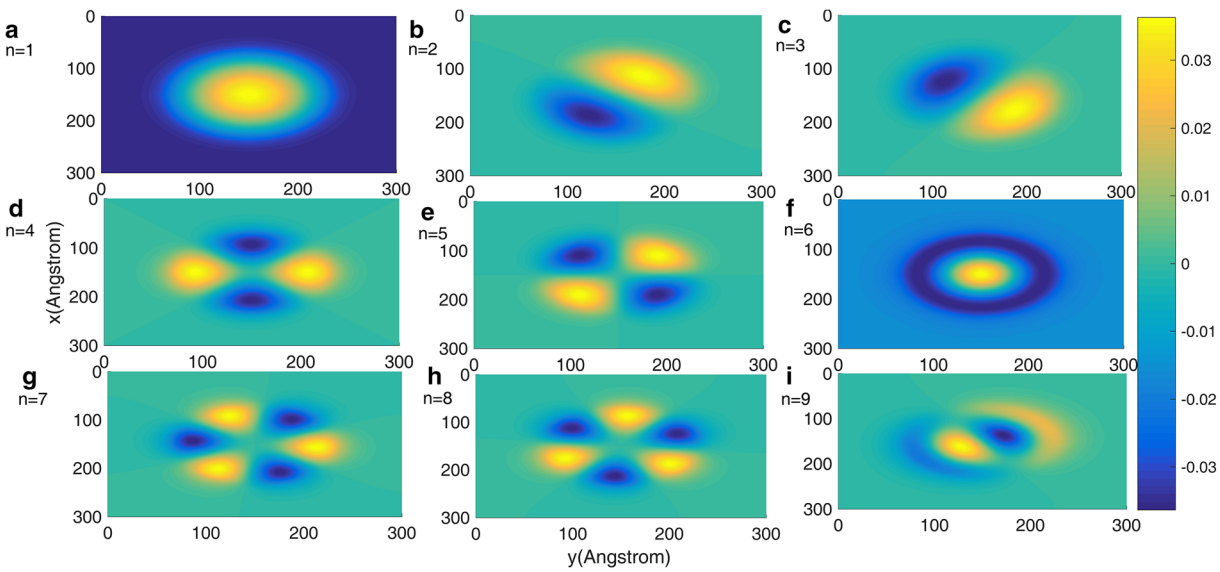


**Fig. 3** Nine lowest eigenfunctions of the circular QD. The state number has been specified on the corresponding panel

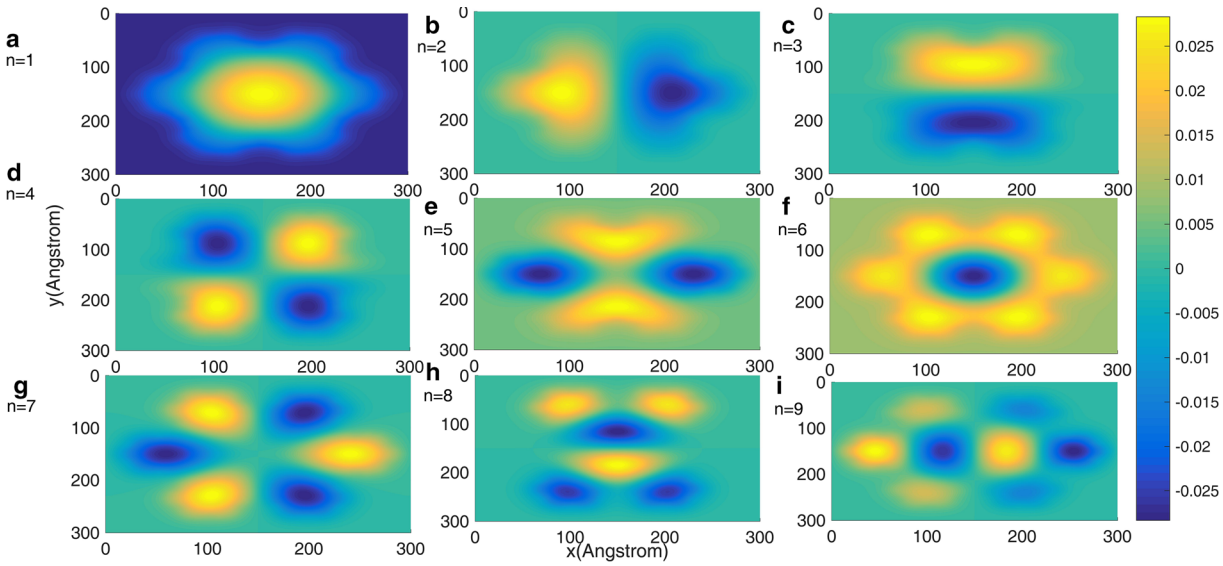


**Fig. 4** Nine lowest eigenfunctions of the snowflake-shaped QD. The state number has been specified on the corresponding panel

eigenfunctions, we have calculated the linear optical absorption coefficient by using Eq. (6).

Now, at first, we compare the nine lowest eigenfunctions of the circular and snowflake-shaped QDs in Figs. 3 and 4. Supposing the panel c of Fig. 2, we assumed the blue region as circular QD and (the blue + yellow) region as Koch-shaped QD. Comparing Figs. 3 and 4 reveals that by changing the QD from circular to snowflake shape, the distribution of the wave function extends to more regions of the assumed rectangular quantum box. But, in both figures, the most of the wave function has been confined in the QD regions. This fact is in agreement with the previous findings (Tiutiunnyk et al. 2014). Another important fact in these figures is that the first and second excited states, as well as the 7th and 8th excited state, are degenerate ones in the circular QDs. However, in the snowflake-shaped QDs, this degeneracy has been breakdown. Besides, we note that by using the snowflake-shaped QDs, we can tune the value of the probability density at different positions in the assumed system.

Now, we study the variation of the absorption coefficient (1/m) as a function of the incident photon energy

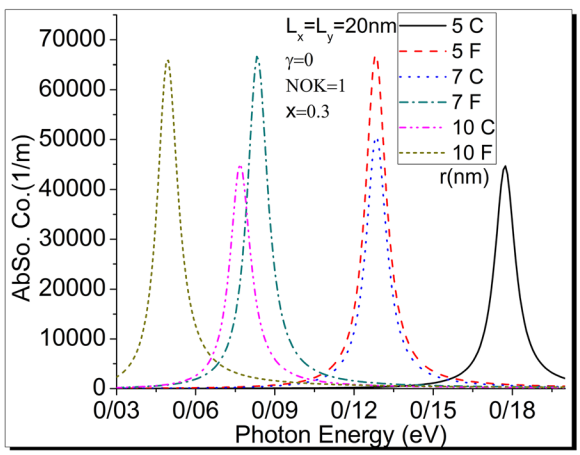


**Fig. 5** Variation of the absorption coefficient (1/m) as a function of the incident photon energy (eV). C and F means circular and snowflake-shaped QDs. Effect of different QD radiuses r has been shown in the figure. NOK means numbers of Koch flakes and γ is the nonparabolicity parameter

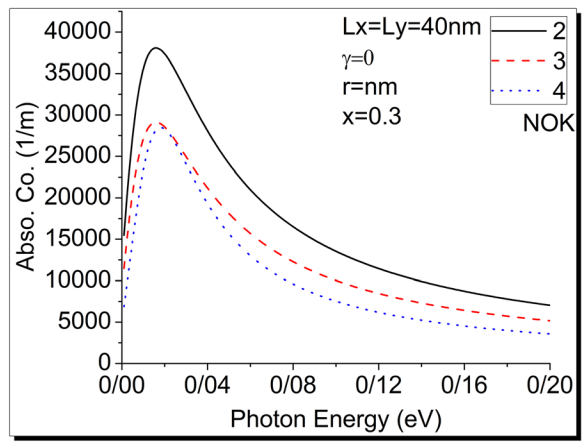


**Fig. 6** Variation of the absorption coefficient (1/m) as a function of the incident photon energy (eV). The effect of different numbers of Koch flakes, NOK, has been shown in the figure. γ and *r* are the nonparabolicity parameter and QD radius, respectively

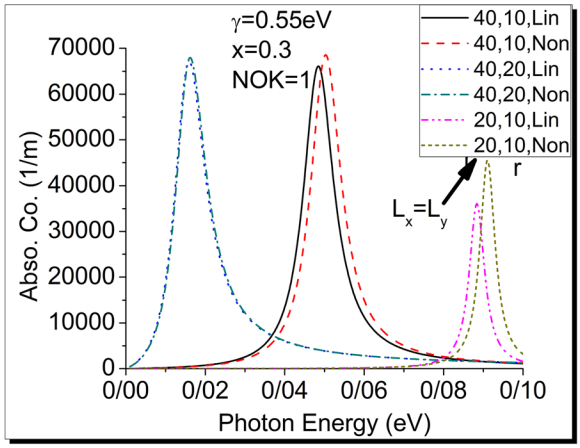


**Fig. 7** Variation of the absorption coefficient (1/m) as a function of the incident photon energy (eV). The effect of different radiuses *r*, as well as the effect of the conduction band nonparabolicity, has been shown in the figure. γ and NOK' are the nonparabolicity parameter and number of Koch snowflakes, respectively. Also "Lin" and "Non" indicate the parabolic and nonparabolic band approximations

(eV) for two circular and snowflake-shaped QDs. The results have been shown in Fig. 5. The letters C and F indicate the circular and snowflake-shaped QDs. In the figure, we also presented the effect of different QD radiuses *r*. As this figure shows, the snowflake-shaped QD has larger absorption coefficients than circular QDs with the same radiuses. Therefore, an experimental researcher should be worried about the circularity of her/his QDs because they have different absorption coefficient (the snowflake-shaped QDs have 1.5 times larger absorption coefficients than circular QDs). Besides, the absorption peak positions shifts toward the lower

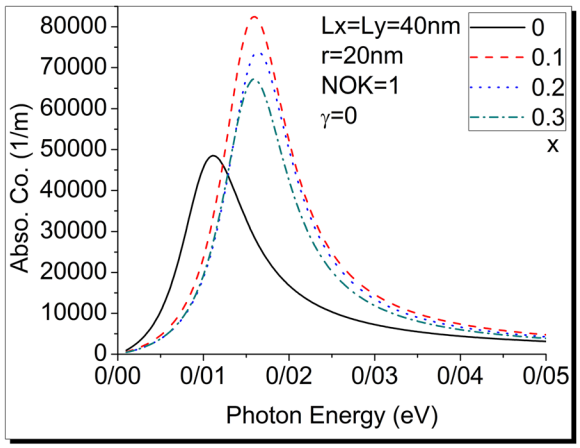


**Fig. 8** Variation of the absorption coefficient (1/m) as a function of the incident photon energy (eV). Effect of different composition parameter *x* has been shown in the figure

energies (i.e., redshift) when the QDs change from circular to snowflake type. However, this is an important parameter in designing optoelectronic devices such as photodetectors or light-emitting devices. We also note that by increasing the QD radius, in both cases of circular and snowflake-shaped ones, the absorption peak positions shift toward the lower energies (i.e., redshift). This fact agrees with the previously published works (Liu and Xu 2008).

In Fig. 6, we have presented the effect of the different numbers of Koch flakes, NOK, on the variation of the absorption coefficient (1/m) as a function of the incident photon energy (eV). However, NOK = 2 means a 2 × 2 array of QDs which are centered at four points ($L_x/4$, $L_y/4$), ($L_x/4$, $3L_y/4$), ($3L_x/4$, $L_y/4$), and ($3L_x/4$, $3L_y/4$). The parameters γ and *r* are also the nonparabolicity parameter and QD radius, respectively. As this figure shows, by increasing the NOK from 2 to 4, the absorption peak positions do not change considerably but the absorption peak amplitude decreases 1.4 times. However, absorption peak amplitude mostly decreased when the NOK changed from 2 to 3, and by further increasing the NOK from 3 to 4, it does not change considerably.

Figure 7 shows the variation of the absorption coefficient (1/m) as a function of the incident photon energy (eV). Effect of two different radiuses "r," two different $L_x = L_y$, and the effect of the conduction band nonparabolicity have been shown in the figure. The parameters γ and NOK indicate the nonparabolicity parameter and number of Koch snowflakes, respectively. Also "Lin" and "Non" indicate the parabolic and nonparabolic band approximations. As this figure shows, at larger QDs or larger system length ($L_x = L_y$), the effect of the nonparabolicity is more negligible. However, the effect of the total system length is more intense. By adding the nonparabolicity effect, we observe that the absorption coefficient increases and this increase is more sensible for systems with larger system length. Also, in the presence of the nonparabolicity effect, the absorption peak positions move toward higher energies (i.e., blueshift).

Another fact is that by increasing the system length, the absorption increases and the corresponding peak position redshifts. Besides by increasing the QD size, in our assumed system, the nonparabolicity effect disappeared and the value of the absorption does not sensibly change and the corresponding peak positions redshifts.

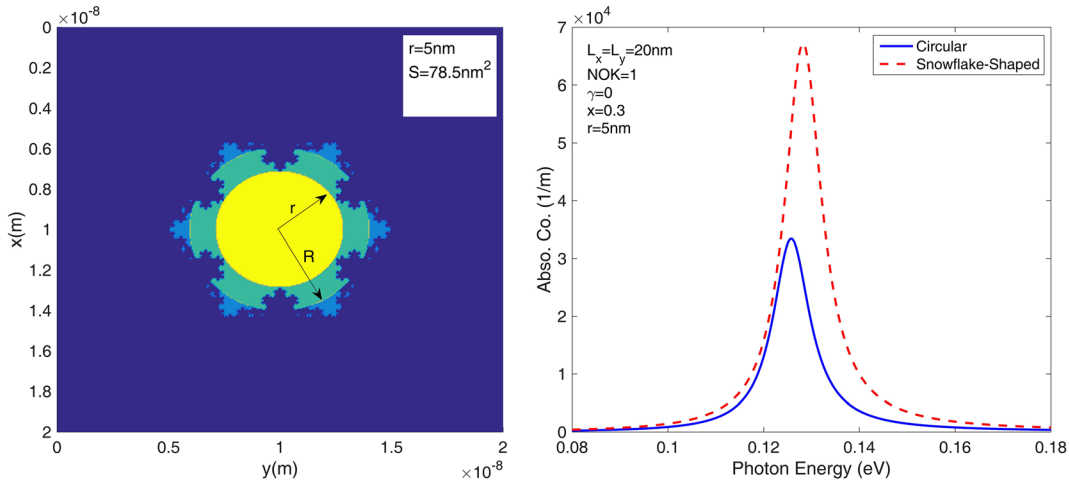


**Fig. 9** Panel **a**: A circular QD with radius $R = 5$ nm and a snowflake-shaped QD with the same area $S = 78.5$ nm. Panel **b**: Variation of the absorption coefficient (1/m) as a function of the incident photon energy (eV) for two circular and snowflake-shaped QDs with same area

In Fig. 8, we consider the effect of the composition parameter x on the absorption coefficient a function of the incident photon energy. We note that larger x lead to larger values of the QD value and therefore directly affect the energy levels, the corresponding eigenfunction, and accordingly affects the absorption coefficient. As this figure shows, by increasing the composition parameter x from 0 to 0.1, absorption amplitude increases and at the same time the absorption peak position blueshifts. But by further increasing the composition parameter x from 0.1 to 0.3, the absorption amplitude decreases, and at the same time, the absorption peak position redshifts. This means tuning of the absorption peak amplitude and position using the composition parameter x can easily be done.

To have a more convincing comparison, we generate a snowflake-shaped QD of the same area with a circular QD. These QDs use the same amount of composing materials. For this purpose, we have provided Fig. 9. Panel a of this figure shows a circular QD with radius $R = 5$ nm and a snowflake-shaped QD with the same area $S = 78.5$ nm. Panel b also shows the variation of the absorption coefficient (1/m) as a function of the incident photon energy (eV) for two circular and snowflake-shaped QDs with the same area. As this panel shows, the snowflake-shaped QD has more than two times greater absorption coefficient than the circular one. The absorption peak position also moves to higher energies (i.e., blueshift) by changing the QD shape from circular to snowflake-shaped one. Thus, we again note that the roundness of the QDs is an important factor in designing the optoelectronic devices.

Finally, we note that by using the snowflake-shaped QDs, we can tune the absorption peak position and peak amplitude. This ability can help experimental physicists to fabricate optoelectronic devices such as photodetectors that works at special wave frequencies and they can manage the intensity of absorption. Another fact is that here we have only changed the geometrical parameters of the system to manage the optical properties of the system. This work may also help to find the desired optical properties in systems that its composing material is not so expensive (i.e., by changing the geometrical parameters in these systems, we may find our desired properties).

## Summary

In this work, we studied the electronic and optical properties of $Al_xGa_{1-x}As/GaAs$ Koch snowflake shape single and multiple QDs. We showed that the snowflake-shaped QDs break down the energy eigenvalue degeneracy of the circular QDs. According to our findings, we propose that an experimental researcher should be worried about the circularity of her/his QDs because the absorption coefficient of the snowflake-shaped QDs can be up to 1.5 times larger than that of a circular QD. Also, the absorption peak positions redshifted when the QDs changed from circular to snowflake type.

For larger QDs or larger system length, the effect of the nonparabolicity could be neglected. The nonparabolicity effect led to a blueshift of the absorption peak positions. Finally, tuning of the absorption peak amplitude and position using the composition parameter x could easily be done.

**Compliance with ethical standards**

**Conflict of interest** The authors declare that they have no conflict of interest.

## References


Adachi S (1985) GaAs, AlAs, and $Al_xGa_{1-x}As$: material parameters for use in research and device applications. J Appl Phys 58:R1–R29

Alemany MMG, Tortajada L, Huang X, Tiago ML, Gallego LJ, Chelikowsky JR (2008) Role of dimensionality and quantum confinement in p-type semiconductor indium phosphide quantum dots. Phys Rev B 78:233101

Allain C, Cloitre M (1986) Optical diffraction on fractals. Phys Rev B 33:3566–3569

Amado M, Domınguez-Adame F, Diez E (2005) Multichannel model of magnetotunneling in disordered electron nanodevices. Physica B 369:293

Amini M, Soleimani M, Ehsani MH (2017) Electronic and optical properties of GaAs/AlGaAs Fibonacci ordered multiple quantum well systems. Superlattice Microst 112:680–687

Anghinolfi L (2012) Self-organized arrays of gold nanoparticles: morphology and plasmonic properties. Springer Science & Business Media

Borri P, Langbein W, Hvam JM, Heinrichsdorff F, Mao M-H, Bimberg D (2000) Spectral hole-burning and carrier-heating dynamics in InGaAs quantum-dot amplifiers. IEEE J Select Top Quant Electron 6:544

Bose C, Midya K, Bose MK (2006) Effect of conduction band non-parabolicity on the donor states in GaAs-(Al, Ga)As spherical quantum dots. Phys E 33:116–119

Bose MK, Midya K, Bose C (2007) Effect of polarization and self-energy on the ground donor state in the presence of conduction band nonparabolicity in GaAs-(Al, Ga)As spherical quantum dot. J Appl Phys 101:054315

Cervenka J, Kosina H, Selberherr S, Zhang J, Hrauda N, Stangl J, Bauer G, Vastola G, Marzegalli A, Montalenti F, Miglio L (2011) Strained MOSFETs on ordered SiGe dots. Solid State Electron 65-66:81–87

Chen Z, Shek CH, Wu CML, Lai JKL (2014) Advances in fractal germanium micro/nanoclusters induced by gold: microstructures and properties. J Nanosci Nanotechnol 14:1318–1337

Dutta Gupta S (1998) Nonlinear optics of stratified media. Prog Opt XXXVIII(1):78

Eah S-K (2011) A very large two-dimensional superlattice domain of monodisperse gold nanoparticles by self-assembly. J Mater Chem 21:16866

Fang T-F, Wang S-J (2007) Cross correlations and shot noise in a Y-shaped quantum dot. J Phys Condens Matter 19:026204

Fussell DP, Hughes S, Dignam MM (2008) Influence of fabrication disorder on the optical properties of coupled-cavity photonic crystal waveguides. Phys Rev B 78:144201

Gerislioglu B, Ahmadivand A (2020) Functional charge transfer plasmon metadevices. Research 2020:9468692

Gerislioglu B, Dong L, Ahmadivand A, Hu H, Nordlander P, Halas NJ (2020a) Monolithic metal dimer-on-film structure: new plasmonic properties introduced by the underlying metal. Nano Lett 20:2087–20493

Gerislioglu B, Bakan G, Ahuja R, Adam J, Mishra YK, Ahmadivand A (2020b) The role of Ge2Sb2Te5 in enhancing the performance of functional plasmonic devices. Mater Today Physics 12:100178

Gonzalez LR, Krupski J, Pietka M, Szwacka T (1999a) Effect of band nonparabolicity on mobility in a d-doped semiconductor. Phys Rev B 60:7768–7771

Gonzalez LR, Krupski J, Pietka M, Szwacka T (1999b) Effect of band nonparabolicity on mobility in a d-doped semiconductor. Phys Rev B 60:7768–7771

Hellström S, Chen Z-H, Fu Y, Qiu M, Soltanmoradi R, Wang Q, Andersson JY (2010) Increased photocurrent in quantum dot infrared photodetector by subwavelength hole array in metal thin film. Appl Phys Lett 96:231110

Hentschel M, Valente DCB, Mucciolo ER, Baranger HU (2007) Improving intrinsic decoherence in multiple-quantum-dot charge qubits. Phys Rev B 76:235309

Ibberson DJ, Bourdet L, Abadillo-Uriel JC, Ahmed I, Barraud S, Calderón MJ, Niquet Y-M, Gonzalez-Zalba MF (2018) Electric-field tuning of the valley splitting in silicon corner dots. Appl Phys Lett 113:053104

Ji LW, Young SJ, Liu CH, Water W, Meen TH, Jywe WY (2008) Nitride-based light-emitter and photodiode dual function devices with InGaN/GaN multiple quantum dot structures. J Cryst Growth 310:2476–2479

Jung K-H, Chang J-S, Kwon Y-S (2006) Two dimensional gold nanodot arrays prepared by using self-organized nanostructure. J Electr Eng Technol 1:246–250

Kasapoglu E, Ungan F, Sari H, Sokmen I, Mora-Ramos ME, Duque CA (2014) Donor impurity states and related optical responses in triangular quantum dots under applied electric field. Superlattice Microst 73:171–184

Kervan N, Altanhan T, Chatterjee A (2003) A variational approach with squeezed-states for the polaronic effects in quantum dots. Phys Lett A 315:280–287

Khordada R (2012) Hydrogenic donor impurity in a cubic quantum dot: effect of position-dependent effective mass. Eur Phys J B 85:114

Le K (2009) Finite element analysis of quantum states in layered quantum semiconductor structures with band nonparabolicity effect. Microw Opt Technol Lett 51:1–5

Lin CY, Ho YK (2011) Photoionization cross sections of hydrogen impurities in spherical quantum dots using the finite-element discrete-variable representation. Phys Rev A 84: 023407

Linares PG, Martí A, Antolín E, Luque A (2011) III-V compound semiconductor screening for implementing quantum dot intermediate band solar cells. J Appl Phys 109:014313

Liu CH, Xu BR (2008) Theoretical study of the optical absorption and refraction index change in a cylindrical quantum dot. Phys Lett A 372:888–892

Liu L, Li Z, Hattori HT, Barbosa CL (2013) Sierpinski Gasket triangular quantum dot lasers, 2013 SBMO/IEEE MTT-S International Microwave & Optoelectronics Conference (IMOC), Rio de Janeiro, p 1–4

Lu YW, Li LY, Liu JF (2018) Influence of surface roughness on strong light-matter interaction of a quantum emitter-metallic nanoparticle system. Sci Rep 8:7115

Ma X, John S (2011) Optical pulse dynamics for quantum-dot logic operations in a photonic-crystal waveguide. Phys Rev A 84:053848

Martinez A, Seoane N, Brown AR, Barker JR, Asenov A (2010) Variability in Si nanowire MOSFETs due to the combined effect of interface roughness and random dopants: a fully three-dimensional NEGF simulation study. IEEE Trans Electr Dev 57:1626–1635

Nilsson HA, Thelander C, Fröberg LE, Wagner JB, Samuelson L (2006) Nanowire-based multiple quantum dot memory. Appl Phys Lett 89:163101

Riffe DM (2002) Temperature dependence of silicon carrier effective masses with application to femtosecond reflectivity measurements. J Opt Soc Am B 19:1092

Rodrıguez AH, Ramırez HY (2008) Analytical calculation of eigen-energies for lens-shaped quantum dot with finite barriers. Eur Phys J B 66:235–238

RVNMelnik1, Willatzen M (2004) Bandstructures of conical quantum dots with wetting layers. Nanotechnology 15:1

Sabzevar M, Ehsani MH, Solaimani M, Ghorbani M (2019) Optical properties of a few semiconducting heterostructures in the presence of Rashba spin-orbit interactions: a two-dimensional finite-difference numerical approach. J Opt Soc Am B 36:1774

Sankar P, Philip R (2018) Nonlinear optical properties of nanomaterials, "Characterization of Nanomaterials, Advances and Key Technologies Micro and Nano Technologies", Chapter 11, p 301–334

Shokri AA, Ebrahiminejad ZH (2011) Spin-dependent tunneling through double-barrier quantum wells with random corrugation interfacial roughness. Phys E 43:1579–1584

Solaimani M (2016) Optical absorption coefficint of GaN/AlN multi-shells quantum dots: optical intensity and magnetic field effects. Optik 127:3934–3939

Solaimani M (2018) Intersubband optical properties of three electrons confined in multishell quantum dots: comparison of two semiconducting compounds. J Comput Electron 17:1135–1142

Solaimani M, Lavaei L, Ghalandari M (2015) Intersubband optical properties of a two electron GaN/AlN constant total effective radius multi-shells quantum rings. Superlattice Microst 82:1–10

Solaimani M, Ghalandari M, Lavaei L (2016) Donor impurity effects on optical properties of GaN/AlN constant total effective radius multishell quantum dots. J Opt Soc America B 33:420

Tiutiunnyk A, Tulupenko V, Mora-Ramos ME, Kasapoglu E, Ungan F, Sari H, Sökmen I, Duque CA (2014) Electron-related optical responses in triangular quantum dots. Phys E 60:127–132

van Veen E, Yuan S, Katsnelson MI, Polini M, Tomadin A (2016) Quantum transport in Sierpinski carpets. Phys Rev B 93:115428

Vargas P, Altbir D (2000) Dipolar effects in multilayers with interface roughness. Phys Rev B 62:6337

Vukovic N, Milanovic V, Radovanovi J (2014) Influence of nonparabolicity on electronic structure of quantum cascade laser. Phys Lett A 378:2222–2225

Yazgan A, Kaya H, Cavdar IH (2015) Optically reconfigurable Sierpinski fractal antennas for RoF based communication systems. Telecommun Syst 59:453–461

Yorulmaz M, Khatua S, Zijlstra P, Gaiduk A, Orrit M (2012) Luminescence quantum yield of single gold nanorods. Nano Lett 12:4385–4391